Princeton Plasma Physics Laboratory

PPPL-5336

Kinetic Simulations of Scrape-Off Layer Physics in the DIII-Tokamak

R.M. Churchill, C.S. Chang, R. Hager, R. Maingi, R. Nazikian, D.P. Stotler

January 2017

Prepared for the U.S. Department of Energy under Contract DE-AC02-09CH11466.

Princeton Plasma Physics Laboratory
Report Disclaimers

Full Legal Disclaimer

Trademark Disclaimer

PPPL Report Availability

Princeton Plasma Physics Laboratory:

http://www.pppl.gov/techreports.cfm

Office of Scientific and Technical Information (OSTI):

http://www.osti.gov/scitech/

Related Links:

U.S. Department of Energy

U.S. Department of Energy Office of Science

U.S. Department of Energy Office of Fusion Energy Sciences

Kinetic simulations of scrape-off layer physics in the DIII-D tokamak

R.M. Churchill[a], J.M. Canik[b], C.S. Chang[a], R. Hager[a], A.W. Leonard[c], R. Maingi[a], R. Nazikian[a], D.P. Stotler[a]

[a] *Princeton Plasma Physics Laboratory, 100 Stellarator Road, Princeton, NJ 08540, USA*
[b] *Oak Ridge National Laboratory, PO Box 2008, Oak Ridge, TN 37831, USA*
[c] *General Atomics, PO Box 85608, San Diego, CA 92186-5608, USA*

Abstract

Simulations using the fully kinetic code XGCa were undertaken to explore the impact of kinetic effects on scrape-off layer (SOL) physics in DIII-D H-mode plasmas. XGCa is a total-f, gyrokinetic code which self-consistently calculates the axisymmetric electrostatic potential and plasma dynamics, and includes modules for Monte Carlo neutral transport. Fluid simulations are normally used to simulate the SOL, due to its high collisionality. However, depending on plasma conditions, a number of discrepancies have been observed between experiment and leading SOL fluid codes (e.g. SOLPS), including underestimating outer target temperatures, radial electric field in the SOL, parallel ion SOL flows at the low field side, and impurity radiation. Many of these discrepancies may be linked to the fluid treatment, and might be resolved by including kinetic effects in SOL simulations.

The XGCa simulation of the DIII-D tokamak in a nominally sheath-limited regime show many noteworthy features in the SOL. The density and ion temperature are higher at the low-field side, indicative of ion orbit loss. The SOL ion Mach flows are at experimentally relevant levels ($M_i \sim 0.5$), with similar shapes and poloidal variation as observed in various tokamaks. Surprisingly, the ion Mach flows close to the sheath edge remain subsonic, in contrast to the typical fluid Bohm criterion requiring ion flows to be above sonic at the sheath edge. Related to this are the presence of elevated sheath potentials,$e\Delta\Phi/T_e \sim 3-4$, over most of the SOL, with regions in the near-SOL close to the separatrix having $e\Delta\Phi/T_e > 4$. These two results at the sheath edge are a consequence of non-Maxwellian features in the ions and electrons there.

1. Introduction

A holistic approach to the plasma exhaust problem is necessary to ensure that in a future magnetic fusion reactor the material surfaces will simultaneously survive harsh plasma conditions and not interfere with core fusing plasma. Many pieces to this puzzle are interdependent, and must be treated simultaneously to understand current experiments and plan future devices and operations.

Key tools currently used for modeling the scrape-off layer (SOL), including the design of future machines such as ITER[1], are fluid transport codes, such as SOLPS[2] and UEDGE[3]. Typical SOL conditions in current experiments would appear to justify the use of a fluid model, as the collisional mean free path in the SOL is less than the parallel connection length, $\lambda < L_\parallel$. However, research has revealed a number of discrepancies between experiment and leading SOL fluid codes (e.g. SOLPS), including underestimating outer target temperatures[4, 5], radial electric field in the SOL[6, 7, 5], parallel ion SOL flows at the low field side[8, 9, 10, 7, 11], and impurity radiation[12, 13]. It was hypothesized by Chankin et. al.[7] that these discrepancies stem from the use of a fluid code, ignoring kinetic effects particularly on parallel transport in the SOL. Specifically he pointed to a chain of causal relations: the code underestimates outer target temperatures, leading to an underestimation of E_r in the SOL, leading to an underestimation of parallel ion flows. Underestimating the target temperature may not be the the underlying cause for all observed discrepancies between experiment and fluid codes, but this thinking highlights the interconnectedness of the scrape-off layer and the need to include as accurate a physics model as possible.

Many kinetic effects could play a role in the SOL, including X-point loss[14], ion orbit loss[15, 16], collisionless high energy particles modifying sheaths[17], non-local transport due to turbulence[18], etc. To correctly model many of these effects requires a kinetic code which spans the closed and open field line regions across the separatrix, and includes realistic SOL physics (kinetic particles, neutrals, sheaths, impurities, etc.) and tokamak geometry (X-point, toroidicity, divertor shape, etc.).

To this end a plan was implemented to simulate SOL physics in a variety of SOL regimes (sheath-limited, high recycling, diverted) using the XGC codes[19, 20, 21], which meet many of the kinetic code criteria discussed in the previous paragraph. These XGC simulations could shed light on the importance and impact of kinetic effects in the SOL. This plan includes making comparisons of XGC results to the fluid code SOLPS.

Email address: rchurchi@pppl.gov (R.M. Churchill)

The results in this paper are from an XGCa simulation of a low density H-mode discharge on the DIII-D tokamak. The rest of the paper is organized as follows: Section 2 describes the XGCa code, including several points important for SOL modeling, Section 3 describes the simulation parameters and discharge parameters, Section 4 discusses several noteworthy simulation results, including main chamber poloidal variation of ion density and temperature, divertor density and temperature comparisons to experiment, SOL parallel flows, and sheath potentials, and Section 5 wraps up with a discussion and details future plans.

2. XGCa

XGCa is a total-*f*, gyrokinetic neoclassical particle-in-cell (PIC) code[19, 20, 21]. The ions are pushed according to a gyrokinetic formalism, and the electrons are drift-kinetic. XGCa is very similar to the more full featured, gyrokinetic turbulence version XGC1[20, 22, 21], the main difference being that XGCa solves only for the axisymmetric electric potential (i.e. no turbulence, hence the "neoclassical" descriptor). An important feature of XGCa is that the electric potential is calculated by solving a gyrokinetic Poisson equation, so that the resulting electric field is self-consistent with the kinetic particles. XGCa also uses a realistic magnetic geometry, created directly from experiment magnetic reconstructions (normally from EFIT EQDSK files), including X-points and material walls.

As this paper is focused on scrape-off layer (SOL) physics, several aspects of XGCa related to its treatment of the SOL are worth mentioning. First, in these simulations a simplified, kinetic, Monte Carlo treatment of neutrals is used (coupling XGCa to the more advanced DEGAS2[23, 24] neutral transport code is ongoing). The simplified neutral routine includes basic neutral processes including electron impact ionization, charge exchange, and elastic collisions. Molecular deuterium is not included. Birth neutrals (D^{0+}) are sampled from a Maxwellian distribution with temperature 3 eV, and source density peaked at a poloidal angle of the X-point, and decaying exponentially in poloidal angle. These neutrals are then launched from fixed ψ_N values in the far-SOL and tracked through neutral collisions, or until lost due to ionization or transferred due to charge exchange. The resulting neutral density and temperature are used to calculate the effect on ion and electron particle distribution functions f_i and f_e due to source rates of ionization and charge exchange. A neutral recycling rate can be specified as input into the code. Impurities have been implemented in a development version of the code, but were not used in these simulations.

The Debye sheath potential at material surfaces isn't prescribed in the simulation, but rather solved for using a modified logical sheath boundary condition, similar to reference [25]. This method avoids resolving the sheath region (which would require a fully kinetic, 6D calculation) while still retaining ion and electron kinetic effects on the sheath potential. Every simulation time step, the sheath potential is adjusted at each wall segment based on the ion and electron particle flux crossing that wall segment, in essence forming a closed-loop feedback system on the sheath potential with a target of ambipolar flux to the wall ($\Gamma_i = \Gamma_e$), with the gain factor an adjustable input to the code. Electrons crossing the simulation boundary with parallel energy $E_\parallel < e\Phi_{sh}$ are reflected back into the plasma. The potential solver uses a boundary condition of zero potential at the sheath-edge, $\Phi_{se} = 0$, i.e. a perfectly floating wall, consistent with the ambipolar flux to the wall. This means the sheath potential is only used for determining the reflection of particles that pass through the sheath edge. It also means in these simulations that the upstream radial electric field (E_r) is not set by Debye sheath potentials ($E_r \sim -3\nabla T_e/e$) but purely by processes such as the thermoelectric force, parallel electron pressure gradient[7], and kinetic effects such as X-point loss[14]. Work is ongoing to incorporate the sheath potential as a boundary condition to the full potential field solver. Work is also ongoing with the more realistic condition of net current to divertor surfaces, though this would require a model for current flow through materials and the private flux region, and modifying cross-field currents to ensure $\nabla \cdot \mathbf{j} = 0$ on a flux surface connected to a material wall in the SOL.

In addition to the $E \times B$ particle drifts calculated from the self-consistent electric potential, XGCa also includes the combined curvature and ∇B magnetic drifts on particle motion. This is important to properly include neoclassical Pfirsch-Schlütter flows.

3. XGCa Simulation Setup

The results presented in this paper are from an XGCa simulation of a low-power H-mode discharge of the DIII-D tokamak[26], shot 153820 at time 3000 ms. This discharge had the following parameters: lower single null (LSN), with the ion ∇B direction towards the lower X-point, $B_0 =$ 2 T, $I_p = 1.1$ MA, $\bar{n}_e = 6.3e19$ m^{-3}, $n_{e,sep} = 1.8e19$ m^{-3}, injected neutral beam power $P_{NBI} = 2.4$ MW, $P_{rad} = 1.3$ MW, $T_{i0} = 2.45$ keV, $T_{e0} = 1.7$ keV, $Z_{eff} = 1.6$, and $H_{98y2} = 1.17$. This discharge was chosen for its lower density, so that the SOL collisionality would be low, where kinetic effects would be expected to be more significant.

The n_e, T_e, and T_i profiles used as input to the code are shown in Figure 1. The recycling rate was set to a low value of $R = 0.95$, with the intention of simplifying the comparison to SOLPS.

The XGCa simulation was run on the Mira supercomputer at Argonne National Laboratory. A total of 524 million electrons and ions were used on the simulation domain. The particle distribution function f velocity grid was 41x42, giving an average of 7.5 particles per velocity space grid. For the unstructured triangulated real space grid, the radial spacing at the low-field side (LFS) midplane averaged $\Delta R \approx 0.5\rho_i$ in the SOL, and less in the

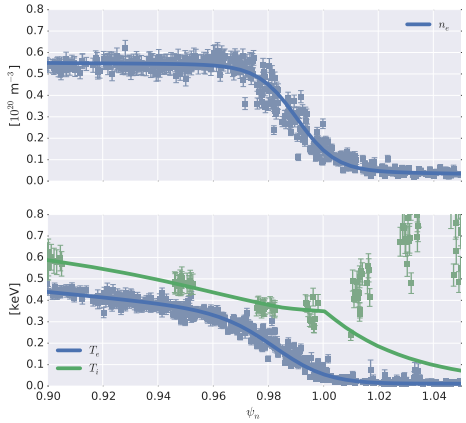

Figure 1: Input profiles to the XGCa simulation. Top plot shows electron density, n_e, with experimental measurements in square markers, and fit in dark solid line, and the bottom plot shows electron temperature, T_e, in blue, and ion temperature, T_i, in green

pedestal region, while the average poloidal spacing across the SOL is $\Delta L_\theta \approx 9\rho_i$. Convergence studies of both the velocity space grid, the real space grid, and time step were performed, showing no significant change in key observables. The final production simulation was run with $\sim 130,000$ CPUs for 24 hours, using a total of $\sim$3 million CPU hours.

4. Results

The following are noteworthy results from the XGCa simulation, with differences from general fluid code results pointed out. More detailed comparisons to SOLPS simulations for the same discharge will be presented in a later paper.

4.1. Density and Ion Temperature

Hot ions executing banana motion in the pedestal region can be lost into the scrape-off layer, and lead to increases in the SOL density and ion temperature, preferentially at the low-field side (LFS)[15, 14, 16]. Plots of the density (since no impurities are used in the simulation, $n_e = n_i$), and ion temperature in normalized poloidal flux (ψ_n) versus poloidal length along a flux surface (L_θ) space are shown in Figure 2. The density has a significant increase in the regions between the X-point and the midplane, at both the low-field side (LFS) and high-field side (HFS), though the LFS increase covers a larger space. The ion temperature is substantially larger at the LFS, peaking $T_{i,sep} \sim 280$ eV at the LFS midplane and dropping to $T_{,sep} = 210$ eV near the top of the machine, rising only slightly at the HFS. This poloidal variation of T_i is similar to the impurity temperature poloidal variation observed on C-Mod[27, 28]. Even larger fractional changes in T_i occur further out in the SOL. A separate DIII-D H-mode XGCa simulation with initial set $T_i \approx T_e$ gave similar poloidal variation, indicating the plasma equilibrium favors this T_i variation in DIII-D H-modes, irrespective of T_i/T_e input (recall XGCa is a total-f code, which evolves the equilibrium). The difference in the poloidal variation of n_i and T_i is suggestive of the fact that the ion orbit loss of higher energy ions is centered closer to the LFS midplane, whereas a larger fraction of ions exit closer to the X-point.

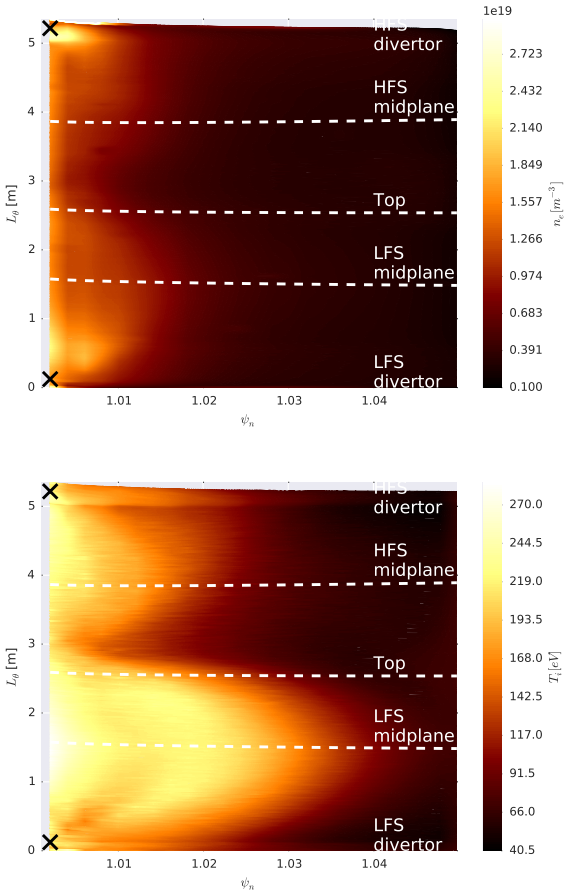

Figure 2: Electron density (top) and ion temperature (bottom) poloidal variation in the SOL. The x-axis is the normalized magnetic flux, ψ_N, and the y-axis is the poloidal distance along a flux surface, L_θ, with 0 at the LFS divertor, increasing poloidally towards the HFS divertor. Recognizable features such as midplane and divertor are marked by the white dashed lines, and the X's on the y-axis indicate where the X-point is.

The substantial T_i variation is the primary cause of an imbalance of simplified total pressure, $p_e + p_i + m_i n_i V_i^2$, in the SOL by more than 50% (n_i variation contributes, but not as strongly. See below for $V_{i,\|}$ variation.). The imbalance of simple pressure is most likely due to ignoring ion viscosity terms, which can be substantial due to temperature anisotropies. Further work is to be done to determine detailed pressure balance, and isolate mechanisms leading to the n_i and T_i increases.

4.2. Comparison to Experiment

Direct comparison of simulated electron density and temperature to the excellent divertor Thomson diagnostic

measurements[29] on DIII-D show that this XGCa simulation overestimates the low-field side divertor T_e, underestimates the LFS divertor n_e, resulting in a decent match to divertor p_e. Note that this is opposite of SOLPS results, which tend to underpredict divertor T_e and overpredict divertor n_e[7]. A plot comparing n_e and T_e from XGCa and divertor Thomson measurements are shown in Figure 3 along the poloidal distance from the LFS divertor, L_θ, in the region $\psi_n = 1.004 - 1.008$. These measurements were accomplished by sweeping the plasma over ~3000 ms past the fixed divertor Thomson views, and mapping to a single time slice at 3000 ms. The nature of this measurement can lead to larger scatter in the data, but still a trend was clearly visible. T_e is about 2x higher in XGCa (30 eV vs 15 eV) and n_e is about 2x lower ($0.9 \times 10^{20} m^{-3}$ vs $1.8 \times 10^{20} m^{-3}$. This overprediction of T_e and underprediction of n_e is present for the the range of flux surfaces where divertor Thomson measurements were available, up to $\psi_n = 1.012$. Divertor radiation (not turned on for this XGCa simulation) is being investigated as a possible mechanism which would bring the simulation and measurements into agreement.

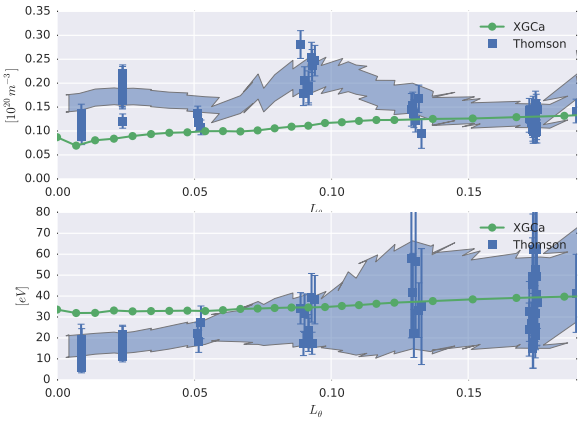

Figure 3: Plots comparing the divertor Thomson measurements of n_e (top) and T_e (bottom) on DIII-D in the region $\psi_n = 1.004 - 1.008$ in blue dots (measurements) and shaded area (fit) to XGCa simulations results at $\psi_n = 1.006$ in green dots. X-point is located at $L_\theta = 0.11$. Shaded area fits are compiled from all measured data, weighted by distance.

4.3. Parallel Ion Flows in the SOL

The parallel ion flow in the SOL plays an important role in impurity migration[10] and particle/heat flux balance to the divertors. The XGCa simulation results for the SOL parallel ion Mach number are shown in Figure 4 ($M_{i,\parallel} = V_{i,\parallel}/c_s$, where $c_s = \sqrt{(T_e + T_i)/m_i}$ is the sound speed). Positive flows (in red) are towards the HFS divertor, negative flows (in blue) are towards the LFS divertor, and white areas are stagnation points.

One of the most notable features of $M_{i,\parallel}$ from Figure 4 is the large values (e.g. $M_{i,\parallel}$~0.5 at the LFS midplane), which is comparable to Mach number measurements in

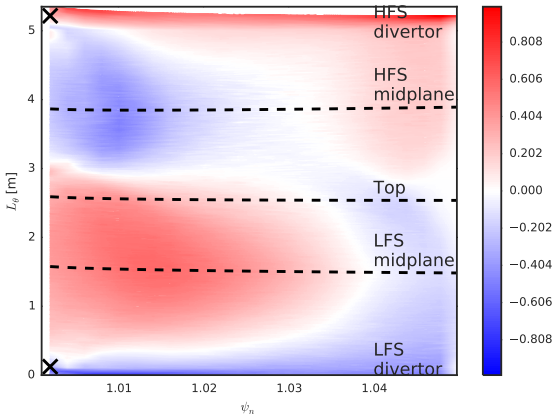

Figure 4: Contour plot of parallel Mach number ($M_{i,\parallel} = V_{i,\parallel}/c_s$) in the SOL. Axes are the same as Figure 2. Color indicates $M_{i,\parallel}$ strength, with red being towards the HFS divertor, and blue towards the LFS divertor. The white points are stagnation points (except next to the left y-axis and next to the top y-axis, which are plotting backgrounds). Recognizable features such as midplane and divertor are marked by the black dashed lines, and the X's on the y-axis indicate where the X-point is.

several tokamaks[10, 9, 11, 7, 30] (most experimental measurements are made in L-mode, due to ease of access for Mach probes, but a few have been made in H-mode[10], which show similar trends and levels of SOL flows). As discussed in the Introduction, many times SOL fluid codes drastically underpredict the SOL parallel ion flows, by factors >3x.

Another notable feature of the XGCa produced SOL flows is the poloidal variation. We can see that in the near-SOL of both the LFS and HFS, the parallel flow is directed towards the opposite side's divertor, reaching a stagnation point just past the top, while in the far-SOL, the flow is directed same side (LFS or HFS) of the plasma. Similar poloidal patterns in the near-SOL were observed in fluid simulations[31], although the magnitude of the simulated flows were lower than measurements on JT-60U. The near-SOL poloidal variation is consistent with the parallel ion flow being dominated by Pfirsch-Schlütter flows[10]. Near the X-point at both the LFS and HFS there is a stagnation point, and the flow changes to be strongly directed towards the respective LFS/HFS divertor, which has been observed on several tokamaks[10], including DIII-D[32]. Note that in L-mode plasmas on C-Mod and JT-60U[33, 10], the HFS parallel flow is mostly directed towards the HFS divertor across the SOL (except in the near-SOL), in contrast to the XGCa results in Figure 4. Experimentally this HFS flow is found to be transport driven[34]. The absence of turbulent transport in the XGCa simulations may explain then this difference in HFS flows. However, an initial comparison to an XGC1 DIII-D H-mode simulation (which self-consistently included electrostatic turbulence across the tokamak) showed qualitatively the same poloidal pattern of the SOL parallel ion flow.

Further investigations into the XGCa results are needed to isolate the separate drivers of the parallel ion flow. However, the main driver which would account for the realistic $M_{i,\parallel}$ levels in XGCa, and which contrasts to fluid codes, would appear to be the radial electric field, E_r, which is solved for using the full gyrokinetic Poisson equation. This would be consistent with work which showed that including the experimentally measured E_r in a simplified equation for the Pfirsch-Schlütter flow recovers the experimentally measured SOL parallel ion Mach number at the LFS midplane[35, 6].

4.4. Elevated Sheath Potentials, Subsonic Sheath flows

The production of a Debye sheath at material surfaces is inherently a kinetic process, with high-energy electrons determining the final sheath potential. Often simplifying assumptions are made to derive a closed form for the normalized sheath potential[36]:

$$\frac{e(\Phi_{se} - \Phi_{wall})}{T_e} = -\frac{1}{2}\ln\left[2\pi\frac{m_e}{m_i}\left(1+\frac{T_i}{T_e}\right)\right] \qquad (1)$$

where Φ_{se} is the electric potential at the sheath edge, and Φ_{wall} is the electric potential at the wall. The normalized sheath potential $(e(\Phi_{se} - \Phi_{wall})/T_e)$ at the LFS divertor plates in XGCa is compared to the expected value from Equation 1 in Figure 5. The XGCa sheath potential is significantly higher than expected, ranging from 3 - 4 over most of the SOL (with near-SOL values approaching 6), while the expected value from Equation 1 for this discharge is almost a constant 2.5 over the entire SOL.

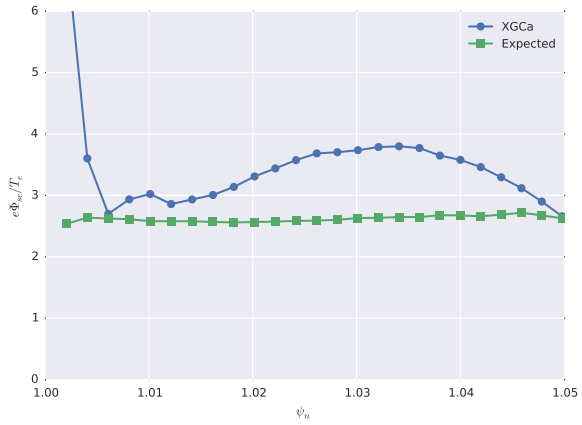

Figure 5: Normalized sheath potential. The XGCa sheath potential is shown in blue circles, the expected sheath potential is shown in green squares.

To understand why the sheath potential is elevated compared to the commonly used analytical Equation 1, we list here the assumptions which are used to derive the analytical equation:

1. Ambipolar flux to material surfaces ($\Gamma_i = \Gamma_e$ for pure plasma)
2. Divertor is electrically isolated (floating), so Φ_{wall} will adjust to incoming flux
3. Ion speed at sheath entrance is a constant, sonic velocity, $V_{se} = c_s$
4. Electrons are Maxwellian in the sheath
5. Electrons follow a Boltzmann relation within the presheath and sheath: $n_e = n_{se}\exp\left[e(\Phi - \Phi_{se})/T_e\right]$

The XGCa sheath routine enforces Item 1, an ambipolar flux. Although Item 2 is not usually satisfied in modern diverted tokamak (most are grounded), this assumption is implicit in the current XGCa sheath routines. The next item to check then is the assumption that ions are sonic at the sheath entrance. The fluid Bohm criterion including $E \times B$ drifts gives[37]:

$$\frac{V_{i,\parallel} + V_{i,\theta}\frac{B_\zeta}{B_\theta}}{c_s} \geq 1 \qquad (2)$$

where $V_{i,\theta}$ is the poldoidal ion velocity, B_ζ and B_θ are toroidal and poloidal magnetic field respectively, and c_s is again the ion sound speed.

This criteria is plotted in Figure 6 both with and without the poloidal drift velocity term. As can be seen, the ions are in fact subsonic, even more so in the regions where the sheath potential is elevated. Including $E \times B$ drifts moves the Mach number up, even satisfying the Bohm criterion at a point in the near-SOL, but overall the flows fall drastically short of the Bohm criterion.

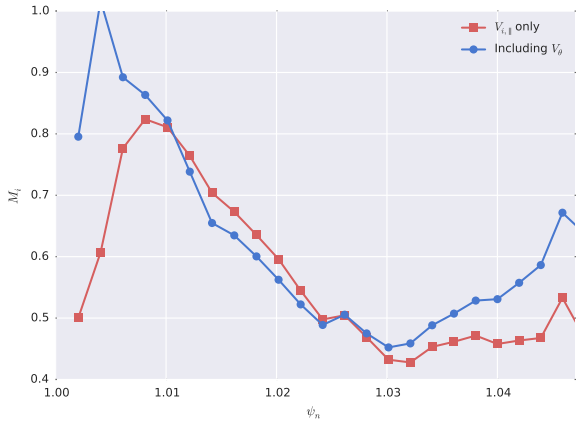

Figure 6: Mach number at the LFS sheath edge. Using only $V_{i,\parallel}$ is shown in red squares, including the effect of $E \times B$ is shown in blue circles. Over most of the SOL, the fluid Bohm criterion is not satisfied.

But how can the ions be subsonic at the sheath entrance, invalidating the fluid Bohm criterion[36]? The derivation of sonic ions at the sheath entrance involves assumptions of monoenergetic ions at a speed $V_i = \sqrt{2e\Phi/m_i}$, and adiabatic electrons through the sheath. However, more general kinetic Debye criterions have been derived, which allow for generic ion (f_i) and electron (f_e) distribution functions at the sheath edge[37, 38, 39]. A common form

for the kinetic Bohm criterion is as follows (see Ref [39] for a good derivation):

$$\frac{1}{m_i}\int d^3v \frac{f_i(\mathbf{v})}{v_\parallel^2} \leq -\frac{1}{m_e}\int d^3v \frac{1}{v_\parallel}\frac{\partial f_e(\mathbf{v})}{\partial v_\parallel} \tag{3}$$

Figure 7 shows the f_i from the XGCa simulation at the sheath edge, near $\psi_n = 1.03$. f_i from the code has a finite T_i, unlike in the ideal Bohm criterion where $f_i(v_\parallel) = \delta(v_\parallel - c_s)$. Unfortunately, the common kinetic Bohm criterion can't be applied to the XGCa distribution functions, since f_i has backwards going ions ($f_i(v_\parallel \leq 0) > 0$), possibly due to neutral ionization, which formally causes Equation 3 to diverge at $v_\parallel = 0$, i.e. the equation implicitly assumes that the sheath absorbs all ions reaching the sheath edge.

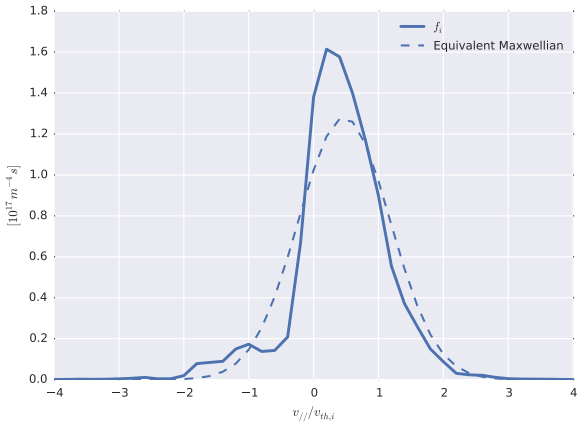

Figure 7: Ion distribution function at the sheath edge, near $\psi_n = 1.03$. f_i from XGCa is shown in solid, and an equivalent Maxwellian (same n_i, T_i and V_i) is shown in dashed lines

Two simple observations can qualitatively account for the elevated sheath potentials, and subsonic flow at the sheath entrance. First, while the electron distribution is close to Maxwellian at the sheath edge, there is a small tail of high energy electrons; these high-energy electrons ultimately determine the sheath potential, with the rest of the electrons being reflected out of the sheath. Second, inspecting f_i in Figure 7, it has a negative skewness, especially when only considering the forward going particles ($v_\parallel > 0$). The *one-way* flux Γ_i^+ of f_i into the sheath is smaller than the one-way flux from an Maxwellian (pictured in Figure 7 with equivalent n_i, V_i, and T_i). This skewed distribution allows for a subsonic $V_{i,\parallel}$ while still satisfying ambipolar flux into the sheath.

A more detailed, quantitative understanding of the kinetic mechanisms generating these distribution functions, and subsequent influence on sheath potentials is ongoing work. It should be pointed out that fluid codes most often assume a value for the sheath potential, and could benefit from an improved model for the sheath potential.

It should be noted that several theories predict subsonic ions at the sheath edge, though at low temperature ($T_i \ll T_e$)[38] and/or low sheath potential plasmas ($e\Phi_{sh} < T_e$)[39], both conditions which aren't met in this discharge. Previous work with a kinetic, 1D2V SOL code[40] over two decades ago observed similar elevated sheath potentials, and subsonic (occasionally supersonic) ions, but sadly this work was not continued, and did not arrive at a final physics understanding of the phenomenon.

5. Conclusion

This work detailed the SOL physics results from an XGCa simulation of a low-density, H-mode discharge on the DIII-D tokamak. The XGC codes are useful for probing kinetic effects in the edge region, including the scrape-off layer, as they include many of the interconnected physics necessary for realistic modelling. The ion density and temperature are larger at the LFS, indicative ion orbit loss from the confined pedestal region. Comparisons of XGCa simulated electron density and temperature to divertor Thomson measurements show an overprediction of LFS target T_e and underprediction of n_e, opposite the typical predictions of fluid codes. The parallel ion Mach number at the LFS midplane reaches experimental levels ($M_i \sim 0.5$), and shows a poloidal variation consistent with the parallel ion flows being dominated by Pfirsch-Schlütter flows, with stagnation points near the X-point at both the LFS and HFS and flows directed towards the divertor below the X-point. The normalized sheath potential at the divertor plates is higher than standard textbook assumptions, along with subsonic ions at the sheath edge, which both implicate kinetic effects in the establishment of the sheath potential in this discharge.

Future work will focus on improvements to the scrape-off layer modelling in XGCa, including the addition of the private flux region, improvements to the boundary conditions in the potential solver, adding impurities, and allowing input anomalous transport as a proxy for turbulence. The comparison to SOLPS simulations of the same discharge will be carried out, and used to more concretely identify differences between kinetic and fluid modelling in the scrape-off layer.

6. Acknowledgements

Special thanks to Dr. Michael Jaworski for his comments on the manuscript. This work supported by the U.S. Department of Energy under DE-AC02-09CH11466, DE-AC05-00OR22725, and DE-FC02-04ER54698. Awards of computer time was provided by the Innovative and Novel Computational Impact on Theory and Experiment (INCITE) program. This research used resources of the Argonne Leadership Computing Facility, which is a DOE Office of Science User Facility supported under contract DE-AC02-06CH11357

[1] A. S. Kukushkin, H. D. Pacher, V. Kotov, G. W. Pacher, D. Reiter, Finalizing the ITER divertor design: The key role of SOLPS modeling, Fusion Eng. Des. 86 (12) (2011) 2865–2873. doi:10.1016/j.fusengdes.2011.06.009.
URL http://dx.doi.org/10.1016/j.fusengdes.2011.06.009

[2] V. Rozhansky, E. Kaveeva, P. Molchanov, I. Veselova, S. Voskoboynikov, D. Coster, G. Counsell, A. Kirk, S. Lisgo, New B2SOLPS5.2 transport code for H-mode regimes in tokamaks, Nucl. Fusion 49 (2) (2009) 025007. doi:10.1088/0029-5515/49/2/025007.
URL http://iopscience.iop.org/article/10.1088/0029-5515/49/2/025007

[3] T. Rognlien, J. Milovich, M. Rensink, G. Porter, A fully implicit, time dependent 2-D fluid code for modeling tokamak edge plasmas, J. Nucl. Mater. 196-198 (1992) 347–351. doi:10.1016/S0022-3115(06)80058-9.
URL http://www.sciencedirect.com/science/article/pii/S0022311506800589

[4] A. V. Chankin, D. P. Coster, R. Dux, C. Fuchs, G. Haas, A. Herrmann, L. D. Horton, A. Kallenbach, M. Kaufmann, C. Konz, K. Lackner, C. Maggi, H. W. Müller, J. Neuhauser, R. Pugno, M. Reich, W. Schneider, SOLPS modelling of ASDEX upgrade H-mode plasma, Plasma Phys. Control. Fusion 48 (6) (2006) 839–868. doi:10.1088/0741-3335/48/6/010.
URL http://iopscience.iop.org/article/10.1088/0741-3335/48/6/010

[5] A. Chankin, D. Coster, Comparison of 2D models for the plasma edge with experimental measurements and assessment of deficiencies, J. Nucl. Mater. 390-391 (2009) 319–324. doi:10.1016/j.jnucmat.2009.01.307.
URL http://www.sciencedirect.com/science/article/pii/S0022311509001238

[6] A. Chankin, D. Coster, N. Asakura, X. Bonnin, G. Conway, G. Corrigan, S. Erents, W. Fundamenski, J. Horacek, A. Kallenbach, M. Kaufmann, C. Konz, K. Lackner, H. Müller, J. Neuhauser, R. Pitts, M. Wischmeier, Discrepancy between modelled and measured radial electric fields in the scrape-off layer of divertor tokamaks: a challenge for 2D fluid codes?, Nucl. Fusion 47 (5) (2007) 479–489. doi:10.1088/0029-5515/47/5/013.
URL http://iopscience.iop.org/article/10.1088/0029-5515/47/5/013

[7] A. V. Chankin, D. P. Coster, G. Corrigan, S. K. Erents, W. Fundamenski, A. Kallenbach, K. Lackner, J. Neuhauser, R. Pitts, Fluid code simulations of radial electric field in the scrape-off layer of JET, Plasma Phys. Control. Fusion 51 (6) (2009) 065022. doi:10.1088/0741-3335/51/6/065022.
URL http://iopscience.iop.org/article/10.1088/0741-3335/51/6/065022

[8] N. Asakura, S. Sakurai, O. Naito, K. Itami, Y. Miura, S. Higashijima, Y. Koide, Y. Sakamoto, Fast measurement of ELM heat and particle fluxes, and plasma flow in the scrape-off layer of the JT-60U tokamak, Plasma Phys. Control. Fusion 44 (5A) (2002) A313–A321. doi:10.1088/0741-3335/44/5A/333.
URL http://iopscience.iop.org/article/10.1088/0741-3335/44/5A/333

[9] S. K. Erents, R. a. Pitts, W. Fundamenski, J. P. Gunn, G. F. Matthews, A comparison of experimental measurements and code results to determine flows in the JET SOL, Plasma Phys. Control. Fusion 46 (11) (2004) 1757–1780. doi:10.1088/0741-3335/46/11/006.
URL http://iopscience.iop.org/article/10.1088/0741-3335/46/11/006

[10] N. Asakura, Understanding the SOL flow in L-mode plasma on divertor tokamaks, and its influence on the plasma transport, J. Nucl. Mater. 363-365 (1-3) (2007) 41–51. doi:10.1016/j.jnucmat.2006.12.029.
URL http://linkinghub.elsevier.com/retrieve/pii/S0022311506006325

[11] M. Groth, J. Boedo, N. Brooks, R. Isler, A. Leonard, G. Porter, J. Watkins, W. West, B. Bray, M. Fenstermacher, R. Groebner, R. Moyer, D. Rudakov, J. Yu, L. Zeng, Effect of cross-field drifts on flows in the main scrape-off-layer of DIII-D L-mode plasmas, Nucl. Fusion 49 (11) (2009) 115002. doi:10.1088/0029-5515/49/11/115002.
URL http://stacks.iop.org/0029-5515/49/i=11/a=115002?key=crossref.8897d227ac5b21e77c83417a36513827

[12] M. Wischmeier, M. Groth, S. Wiesen, S. Potzel, L. Aho-Mantila, D. P. Coster, R. Dux, C. Fuchs, a. Kallenbach, H. W. Müller, D. Reiter, a. Scarabosio, Assessment of edge modeling in support of ITER, J. Nucl. Mater. 415 (1 SUPPL) (2011) S523–S529. doi:10.1016/j.jnucmat.2011.02.020.
URL http://dx.doi.org/10.1016/j.jnucmat.2011.02.020

[13] J. M. Canik, a. R. Briesemeister, C. J. Lasnier, a. W. Leonard, J. D. Lore, a. G. McLean, J. G. Watkins, Modeling of detachment experiments at DIII-D, J. Nucl. Mater. 463 (2015) 569–572. doi:10.1016/j.jnucmat.2014.11.077.
URL http://dx.doi.org/10.1016/j.jnucmat.2014.11.077

[14] C. S. Chang, S. Kue, H. Weitzner, X-transport: A baseline non-ambipolar transport in a diverted tokamak plasma edge, Phys. Plasmas 9 (9) (2002) 3884. doi:10.1063/1.1490348.

[15] K. C. Shaing, Ion orbit loss and poloidal plasma rotation in tokamaks, Phys. Fluids B Plasma Phys. 4 (1) (1992) 171. doi:10.1063/1.860430.
URL http://link.aip.org/link/PFBPEI/v4/i1/p171/s1&Agg=doi$\delimiter"026E30F$nhttp://link.aip.org/link/PFBPEI/v4/i10/p3310/s1&Agg=doi

[16] W. Stacey, Effect of ion orbit loss on distribution of particle, energy and momentum sources into the tokamak scrape-off layer, Nucl. Fusion 53 (6) (2013) 063011. doi:10.1088/0029-5515/53/6/063011.
URL http://stacks.iop.org/0029-5515/53/i=6/a=063011?key=crossref.932606ef6638b7c215dafad3cb5bba44

[17] J. A. Wesson, Effect of temperature gradient on plasma sheath, Plasma Phys. Control. Fusion 37 (12) (1995) 1459–1466. doi:10.1088/0741-3335/37/12/008.
URL http://iopscience.iop.org/article/10.1088/0741-3335/37/12/008

[18] J. T. Omotani, B. D. Dudson, Non-local approach to kinetic effects on parallel transport in fluid models of the scrape-off layer, Plasma Phys. Control. Fusion 55 (5) (2013) 055009. doi:10.1088/0741-3335/55/5/055009.
URL http://stacks.iop.org/0741-3335/55/i=5/a=055009?key=crossref.bcf85ab52246c588d8cb878768cc598d

[19] R. Hager, C. S. Chang, Gyrokinetic neoclassical study of the bootstrap current in the tokamak edge pedestal with fully nonlinear Coulomb collisions, Phys. Plasmas 23 (4) (2016) 042503. doi:10.1063/1.4945615.
URL http://scitation.aip.org/content/aip/journal/pop/23/4/10.1063/1.4945615

[20] S. Ku, C. Chang, P. Diamond, Full-f gyrokinetic particle simulation of centrally heated global ITG turbulence from magnetic axis to edge pedestal top in a realistic tokamak geometry, Nucl. Fusion 49 (11) (2009) 115021. doi:10.1088/0029-5515/49/11/115021.
URL http://iopscience.iop.org/0029-5515/49/11/115021

[21] S. Ku, R. Hager, C. Chang, J. Kwon, S. Parker, A new hybrid-Lagrangian numerical scheme for gyrokinetic simulation of tokamak edge plasma, J. Comput. Phys. 315 (2016) 467–475. doi:10.1016/j.jcp.2016.03.062.
URL http://linkinghub.elsevier.com/retrieve/pii/S0021999116300274

[22] C. S. Chang, S. Ku, P. Diamond, M. Adams, R. Barreto, Y. Chen, J. Cummings, E. D'Azevedo, G. Dif-Pradalier, S. Ethier, L. Greengard, T. S. Hahm, F. Hinton, D. Keyes, S. Klasky, Z. Lin, J. Lofstead, G. Park, S. Parker, N. Podhorszki, K. Schwan, A. Shoshani, D. Silver, M. Wolf, P. Worley, H. Weitzner, E. Yoon, D. Zorin, Whole-volume integrated gyrokinetic simulation of plasma turbulence in realistic diverted-tokamak geometry, J. Phys. Conf. Ser. 180 (1) (2009) 012057. doi:10.1088/1742-6596/180/1/012057.
URL http://iopscience.iop.org/article/10.1088/1742-6596/180/1/012057

[23] D. Stotler, C. Karney, Neutral Gas Transport Modeling with DEGAS 2, Contrib. Plasma Phys. 34 (2-3) (1994) 392–397. doi:10.1002/ctpp.2150340246.

[24] D. P. Stotler, C. S. Chang, G. Park, S. H. Ku, Energy

conservation tests of a coupled kinetic plasma kinetic neutral transport code, Comput. Sci. Discov. 6 (1) (2013) 015006. doi:10.1088/1749-4699/6/1/015006.
URL http://iopscience.iop.org/1749-4699/6/1/015006/article/

[25] S. Parker, R. Procassini, C. Birdsall, B. Cohen, A Suitable Boundary Condition for Bounded Plasma Simulation without Sheath Resolution, J. Comput. Phys. 104 (1) (1993) 41–49. doi:10.1006/jcph.1993.1005.
URL http://www.sciencedirect.com/science/article/pii/S0021999183710053

[26] J. L. Luxon, T. C. Simonen, R. D. Stambaugh, Overview of the DIII-D Fusion Science program, Fusion Sci. Technol. 48 (2) (2005) 807–827.

[27] C. Theiler, R. M. Churchill, B. Lipschultz, M. Landreman, D. R. Ernst, J. W. Hughes, P. J. Catto, F. I. Parra, I. H. Hutchinson, M. L. Reinke, A. E. Hubbard, E. S. Marmar, J. T. Terry, J. R. Walk, Inboard and outboard radial electric field wells in the H-and I-mode pedestal of Alcator C-Mod and poloidal variations of impurity temperature, Nucl. Fusion 54 (8) (2014) 083017. doi:10.1088/0029-5515/54/8/083017.
URL http://stacks.iop.org/0029-5515/54/i=8/a=083017

[28] R. M. Churchill, C. Theiler, B. Lipschultz, I. H. Hutchinson, M. L. Reinke, D. Whyte, J. W. Hughes, P. Catto, M. Landreman, D. Ernst, C. S. Chang, R. Hager, A. Hubbard, P. Ennever, J. R. Walk, Poloidal asymmetries in edge transport barriersa), Phys. Plasmas 22 (5) (2015) 056104. doi:10.1063/1.4918353.
URL http://scitation.aip.org/content/aip/journal/pop/22/5/10.1063/1.4918353

[29] T. N. Carlstrom, C. L. Hsieh, R. Stockdale, D. G. Nilson, D. N. Hill, Initial operation of the divertor Thomson scattering diagnostic on DIII-D, Rev. Sci. Instrum. 68 (2) (1997) 1195. doi:10.1063/1.1147893.
URL http://scitation.aip.org/content/aip/journal/rsi/68/2/10.1063/1.1147893

[30] J. Boedo, Edge turbulence and SOL transport in tokamaks, J. Nucl. Mater. 390-391 (2009) 29–37. doi:10.1016/j.jnucmat.2009.01.040.
URL http://www.sciencedirect.com/science/article/pii/S0022311509000531

[31] N. Asakura, H. Takenaga, S. Sakurai, G. Porter, T. Rognlien, M. Rensink, K. Shimizu, S. Higashijima, H. Kubo, Driving mechanism of SOL plasma flow and effects on the divertor performance in, Nucl. Fusion 44 (4) (2004) 503–512. doi:10.1088/0029-5515/44/4/004.
URL http://stacks.iop.org/0029-5515/44/i=4/a=004?key=crossref.7dc421e0b53c3a8adf8882974b12cbbd

[32] J. Boedo, R. Lehmer, R. Moyer, J. Watkins, G. Porter, T. Evans, A. Leonard, M. Schaffer, Measurements of flows in the DIII-D divertor by Mach probes, J. Nucl. Mater. 266-269 (1999) 783–787. doi:10.1016/S0022-3115(98)00549-2.
URL http://www.sciencedirect.com/science/article/pii/S0022311598005492

[33] B. LaBombard, J. Rice, A. Hubbard, J. Hughes, M. Greenwald, J. Irby, Y. Lin, B. Lipschultz, E. Marmar, C. Pitcher, N. Smick, S. Wolfe, S. Wukitch, t. A. Group, Transport-driven Scrape-Off-Layer flows and the boundary conditions imposed at the magnetic separatrix in a tokamak plasma, Nucl. Fusion 44 (10) (2004) 1047–1066. doi:10.1088/0029-5515/44/10/001.
URL http://iopscience.iop.org/article/10.1088/0029-5515/44/10/001

[34] N. Smick, B. Labombard, I. H. Hutchinson, Transport and drift-driven plasma flow components in the Alcator C-Mod boundary plasma, Nucl. Fusion 53 (53) (2013) 23001–26. doi:10.1088/0029-5515/53/2/023001.
URL http://iopscience.iop.org/0029-5515/53/2/023001

[35] R. A. Pitts, J. Horacek, T. C. V. Team, Neoclassical and transport driven parallel SOL flows on TCV, Europhys. Conf. Abstr. 31F (July) (2007) 2–5.

[36] P. Stangeby, The Plasma Boundary of Magnetic Fusion Devices, Institute of Physics Publishing, Bristol, 2000.

[37] P. C. Stangeby, a. V. Chankin, The ion velocity (BohmChodura) boundary condition at the entrance to the magnetic presheath in the presence of diamagnetic and EB drifts in the scrape-off layer, Phys. Plasmas 2 (1995) (1995) 707. doi:10.1063/1.871421.

[38] J. Loizu, P. Ricci, C. Theiler, Existence of subsonic plasma sheaths., Phys. Rev. E. Stat. Nonlin. Soft Matter Phys. 83 (1 Pt 2) (2011) 016406. doi:10.1103/PhysRevE.83.016406.
URL http://www.ncbi.nlm.nih.gov/pubmed/21405783

[39] S. D. Baalrud, B. Scheiner, B. Yee, M. Hopkins, E. Barnat, Extensions and applications of the Bohm criterion, Plasma Phys. Control. Fusion 57 (4) (2015) 044003. doi:10.1088/0741-3335/57/4/044003.
URL http://iopscience.iop.org/article/10.1088/0741-3335/57/4/044003

[40] O. V. Batishchev, S. I. Krasheninnikov, P. J. Catto, A. A. Batishcheva, D. J. Sigmar, X. Q. Xu, J. A. Byers, T. D. Rognlien, R. H. Cohen, M. M. Shoucri, I. P. Shkarofskii, Kinetic effects in tokamak scrape-off layer plasmas, Phys. Plasmas 4 (5) (1997) 1672. doi:10.1063/1.872280.
URL http://scitation.aip.org/content/aip/journal/pop/4/5/10.1063/1.872280

PPPL PRINCETON PLASMA PHYSICS LABORATORY

Princeton Plasma Physics Laboratory
Office of Reports and Publications

Managed by
Princeton University

under contract with the
U.S. Department of Energy
(DE-AC02-09CH11466)

P.O. Box 451, Princeton, NJ 08543
Phone: 609-243-2245
Fax: 609-243-2751

E-mail: publications@pppl.gov

Website: http://www.pppl.gov